EXPERIMENTAL AND NUMERICAL INVESTIGATION OF PLASTIC HINGING OF FASTENERS IN CLT BALLOON-FRAME CONNECTIONS: INSIGHTS FROM THE WOODWISE LARGE-SCALE COMPARTMENT FIRE TESTS

Nicolas Coello[1], Erica C. Fischer[2], David Barber[3], Laura Hasburgh[4], Kara Yedinak[5]

ABSTRACT

Connections in mass timber buildings degrade during fire due to charring and temperature-dependent material reduction, leading to significant fastener deformation. This study develops a temperature-dependent Beam-on-Foundation (BoF) formulation for CLT balloon-frame connections exposed to the WOODWISE large-scale compartment fire. The ambient-temperature BoF model was first validated against embedment and single-shear tests from the literature, followed by development and validation of a heat transfer model using thermocouple data from WOODWISE Test #3. The validated temperatures were sequentially coupled to the mechanical model, incorporating temperature-dependent degradation and progressive removal of timber springs to represent charring. Results show that the predicted global force–displacement response follows the increase in char depth and spring removal. The framework also provides local force–deformation and stress–strain histories, enabling investigation of thermo-mechanical degradation mechanisms in CLT connections under fire.

Keywords: Beam-on-Foundation modelling; CLT connections; compartment fire.

1 INTRODUCTION

During a fire, connections play a crucial role in the structural integrity of mass timber buildings. Failure of fasteners within connections can compromise both fire compartmentation and structural stability while large deformations in or at the connection during a fire can impose deformations on the unexposed portions of the building. Mass timber connections (e.g., glue laminated (glulam) beam-to-column connections and within cross laminated timber (CLT) balloon and platform frame connections) often consist of steel plates or angles connected to the timber with screws. As the exposed timber chars, the mechanical properties are lower than the uncharred timber. When a screw within a connection is partially within charred and uncharred timber, the applied forces can result in shear plastic hinges forming within the fastener. The hinge can occur at the unexposed surface of the steel connection plate, or at the interface between the charred timber and uncharred timber [1 – 3]. The formation of these plastic hinges results in substantial deformation of the connections that may not be accounted for in structural design. Recent studies observed deformations of self-tapping screw

[1] Graduate Research Assistant, Oregon State University,
e-mail: coelloce@oregonstate.edu
[2] Associate Professor, Oregon State University,
e-mail: erica.fischer@oregonstate.edu
[3] Principal, Arup
e-mail: david.barber@arup.com
[4] Materials Research Engineer, Forest Products Laboratory, United States Forest Service
e-mail: laura.e.hasburgh@usda.gov
[5] Forest Products Technologist, Forest Products Laboratory, United States Forest Service
e-mail: kara.yedinak@usda.gov

fasteners within glulam beam-to-column connections and within CLT balloon and platform frame connections during the heating phase of the fire [1 – 3].

Current prescriptive fire design focus on maintaining load-carrying capacity of the connection and preventing temperature rises within the connection. However, the ability of the connection to prevent fire integrity failure is going to depend upon the deformations within the connection. These deformations are related to fastener bending, plastic hinge formation, or progressive redistribution of stresses along the fastener.

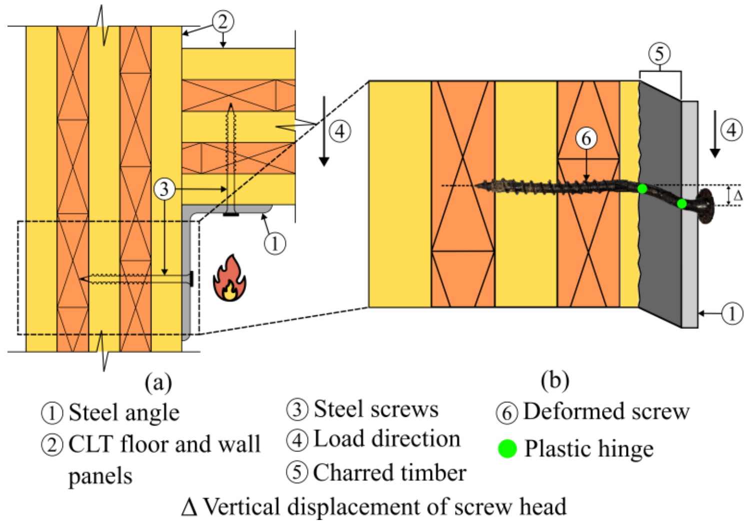

Figure 1. Balloon-frame connection from WOODWISE experiments. (a) Connection configuration. (b) Plastic hinging of wall screws as char layer forms.

Figures 1 & 2 show plastic hinging of 5.6 mm diameter screws in a wall-to-floor balloon-frame connection, as observed in the WOODWISE fire experiments [4]. Two distinct plastic hinges were identified in this screw: the first at a depth of 45 mm from the exposed surface, and the second at the interface between the steel angle and the timber surface (i.e., 10 mm deep from the exposed surface), where combined bending and bearing stresses were present on the screw. This failure mode supports the need for models capable of simulating temperature-dependent steel screw yielding and the progressive loss of wood embedment due to charring. These connections were subjected only to their self-weight, estimated to be approximately 12 kg, with no additional structural gravity loading applied.

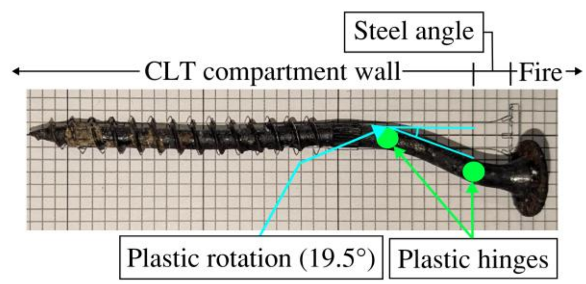

Figure 2. Failure mode of steel fastener.

The Beam-on-Foundation (BoF) framework provides a robust numerical approach for analysing dowel-type timber connections, offering an advanced alternative to rigid-plastic methods such as the European Yield Model (EYM). The fastener is modelled as a deformable beam, while the timber is represented by discrete nonlinear springs acting as the "foundation" [5–7].

This approach is advantageous for engineered products like CLT, as spring properties can be assigned by layer to distinguish grain orientations. By capturing nonlinear material behaviour, the BoF model reproduces load–displacement response with significantly lower computational demand than full 3D continuum FE models [22]. Although widely applied at ambient temperature [5,6], it has not been implemented at high temperatures.

The objectives of this research are to therefore to (i) develop a temperature-dependent BoF modelling framework that adapts existing connection theory to CLT in order to predict plastic hinging and fastener deformation during fire, (ii) assess the viability of this model against experimental results developed during the WOODWISE experiments.

2 METHODOLOGY

The mechanical BoF model is validated at ambient temperature using embedment strength and single-shear connection experiments from the literature. The ambient BoF model is adapted for a coupled thermal-stress based analysis by coupling with a heat transfer model. The authors validated their heat transfer modelling methodologies against experimental thermocouple measurements from the WOODWISE experiments as well as independent fire experiments on steel elements reported in the literature.

2.1 Beam-on-Foundation model validation

The mechanical interaction between the fastener and timber in the BoF model is characterized through embedment behaviour, with yielding commonly interpreted using Johansen's European Yield Theory [30]. At ambient conditions, embedment strength depends on timber density, fastener diameter, and grain direction [13]. A parameterized nonlinear slip model [18,19] was adopted, introducing parameter a_1 to control the transition between elastic and plastic response. A simplified formulation was used to define the stress–strain response of the fastener and the force–displacement response of the timber springs, with the elastic portion governed by k_{el} and the plastic portion by the parametric curve (Figure 3).

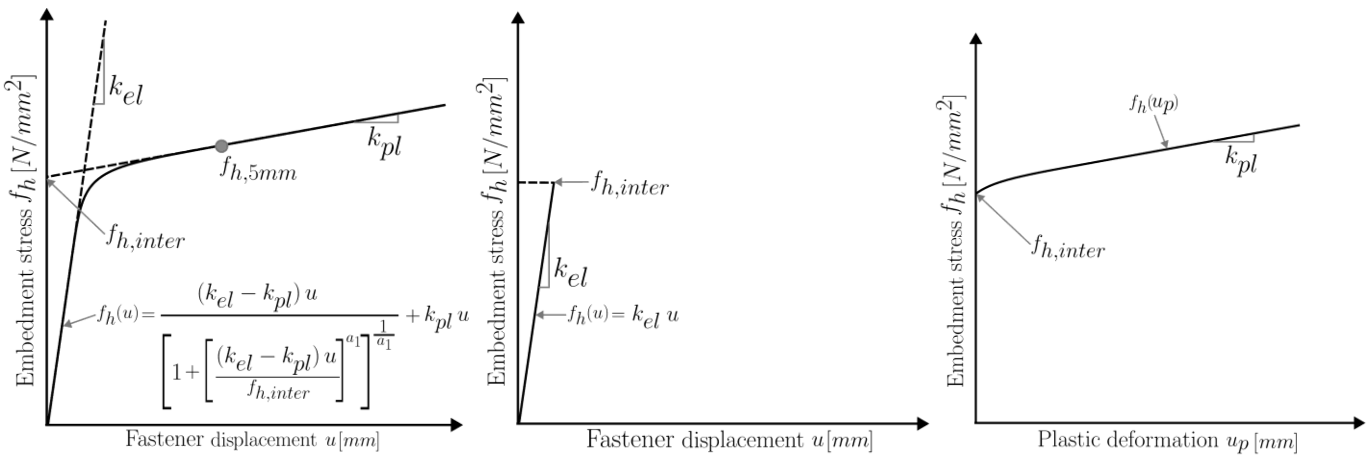

Figure 3. a) Full parametric curve. b) Elastic portion simplification. c) Plastic portion using parametric curve values

To validate the mechanical model, two embedment experiments and one previously validated BoF model were replicated, including both solid timber and CLT configurations. Parameters were derived from the literature [20,25], with k_{el} defined as the slope between 10% and 40% of the embedment stress at 5 mm $f_{h,5mm}$ or peak stress. Table 1 summarizes the literature used for validation.

Table 1. Validation models developed

Model	Input/Validation	Case modelled	Diameter [mm]	Thickness [mm]	Reference
BoF1	Solid timber/CLT	$f_{e,0,clt}$, $f_{e,0,st}$	8	60	[27]
BoF2	CLT/CLT	F-10-0.33-0	10	60	[28]
BoF3	Solid timber/CLT	5.1.3	12	90	[26]

Although the plastic modulus k_{pl} has been previously defined as the slope of the stress–displacement curve between displacements corresponding to 0.5 and 1.5 times the fastener diameter, the experiments considered in this study did not reach these displacements. In BoF3, the maximum displacement did not exceed 0.5 times the diameter. Consequently, using fractions of the diameter was not feasible. Instead, k_{pl} was defined as the slope of the stress–displacement curve over the final portion of the response, expressed as a fraction of the maximum recorded displacement. Specifically, the slope was computed between 0.9 and 1.0 times the maximum displacement.

The parameter a_1 controls the slope of the transition between k_{el} and k_{pl}. Lower values produce a nonlinear transition, whereas higher values result in a sharper change in slope, approaching a bilinear response. The parameter a1 was adjusted to the experiment curve using a Mean Square Error (MSE) method.

In a BoF system, a characteristic length L_c, dependent on both the fastener stiffness and the foundation stiffness, can be calculated as described in [21]. Previous studies have used a fraction of L_c to define the mesh size and to evaluate the accuracy of the BoF model as a function of this ratio [29]. In the present study, the timber spring spacing s_{TS} was defined as $0.3L_c$.

For BoF3, the steel angle attached by the fastener was modelled using linear steel springs spaced at $s_{SS} = 4\ mm$. All models were performed using a quasi-static monotonic displacement-controlled loading protocol with a linearly ramped imposed displacement. Figure 4 shows a schematic of the model setup for BoF1 – BoF3.

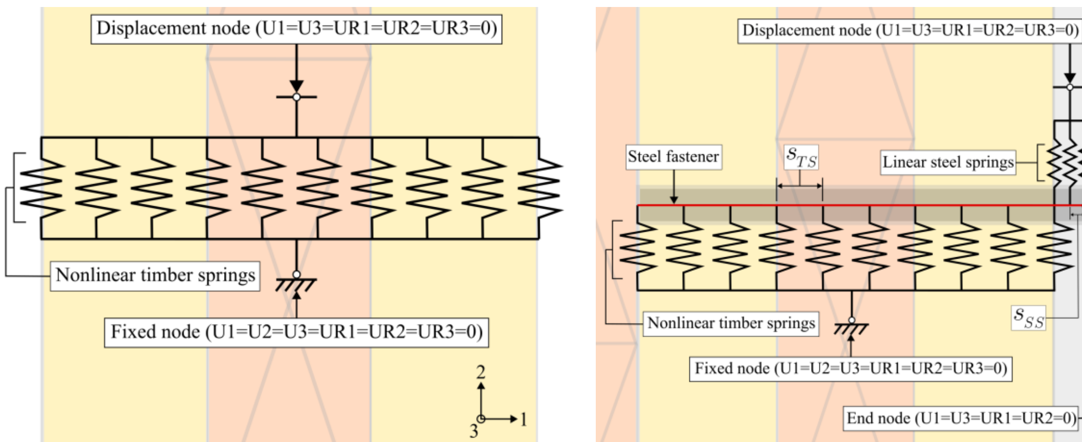

a) b)

Figure 4. BoF ambient temperature models. a) BoF1 – BoF2. b) BoF3.

2.2 Expansion of BoF model for thermal-stress analysis

Steel fasteners, due to their high thermal conductivity, act as heat conduits, transferring heat deep into the timber cross-section and accelerating charring at the steel-timber interface [7 – 9]. To simulate this effect on the mechanical behaviour of the connection, finite element (FE) heat transfer models were employed to predict temperature distributions [9,10]. These models accounted for transient heat conduction within the steel and timber components as well as convection, and radiation at exposed surfaces. In this study, a heat transfer model was developed to predict the temperature distribution within the connection. The resulting temperature time histories were then used as input to an extended BoF model, in which the mechanical properties of each discretized component were updated as a function of temperature to simulate thermo-mechanical degradation throughout the fire exposure. The developed model setup followed the single-shear configuration presented in Figure 4(b).

2.2.1 *Heat transfer model validation*

The gas temperature was characterized by the temperature-time obtained from the WOODWISE Test #3 [4] and is presented in Figure 5(a). The wall panel section was a five-ply Southern Yellow Pine CLT. The steel fasteners consisted of Simpson Strong-Tie® SDWS™ 127 mm structural wood screws with diameter 5.6 mm. The steel fastener attached an A36 steel angle measuring 152 mm × 101 mm × 9.5 mm. The steel fastener was modelled as a two-dimensional domain discretized along its length and across its diameter. A convective heat transfer coefficient of 25 $\frac{W}{m^2K}$ and a radiation emissivity of 0.7 were used at the surface of the connection in contact with the fire. The thermal properties of CLT were taken from EC5 [14] and thermal properties of the steel were from EC3 [15]. These temperature-dependent properties are calibrated for standard fire exposure conditions and may not fully capture material behaviour under non-standard fire scenarios; however, they were adopted due to the absence of alternative validated datasets. Figure 5(b) illustrates the heat transfer mesh configuration and identifies the nodes corresponding to thermocouple locations, where experimental temperature measurements were available at depths ranging from 0 to 124 mm from the exposed surface. To validate the heat transfer modelling methodology, the results from the heat transfer model were compared against the experimental data.

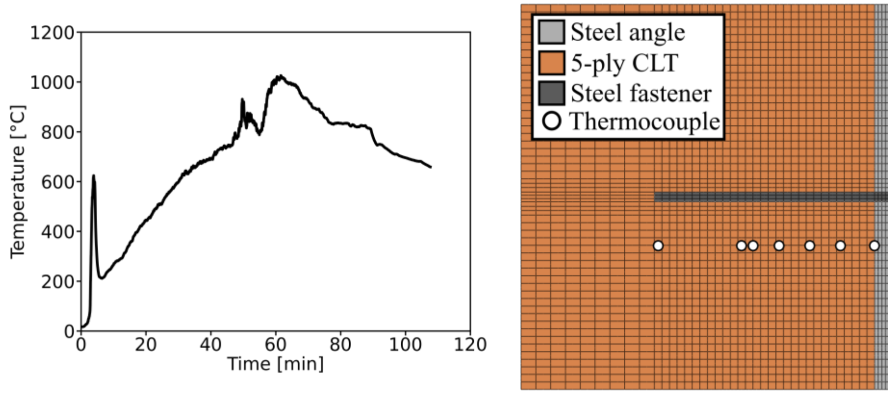

Figure 5. a) Gas temperature used as input for heat transfer model. b) Heat transfer model mesh, elements, and thermocouple locations.

2.2.2 *Expanded BoF model: Sequentially coupled thermal-stress analysis*

With the transient temperature field validated, the thermal response was sequentially coupled to the mechanical formulation of the BoF model. In this approach, the temperature time history obtained from the heat transfer analysis was mapped to each discretized spring element representing the timber and steel elements. Temperature-dependent steel material properties were simulated using retention factors from EC3 [15]. Mechanical properties of timber springs were estimated through temperature-dependent density from EC5 [14] and density-dependent expressions used from literature [22]. Mechanical properties were updated at each time increment according to the temperature-dependent degradation relationships mentioned, enabling simulation of the evolving thermo-mechanical behaviour of the connection throughout fire exposure. This sequential coupling assumes one-way interaction, where the thermal field influences the mechanical response without feedback to the heat transfer analysis. The elastic modulus k_{el} of the timber springs was calculated using the regression model reported in [20]. The embedment strength $f_{h,inter}$ of the timber springs was calculated using the expression for screws reported in [31]. The plastic modulus k_{pl} was calculated from a regression model in [22]. The timber springs were spaced at $7\ mm$, corresponding to $0.31L_c$. Table 2 summarizes the resulting

Table 2. Mechanical properties used for timber springs

Load-to-grain angle	$K_{el}[N/mm]$	$F_{h,inter}[N]$	$K_{pl}[N/mm]$
0°	1343	1253	30
90°	554	1253	100

mechanical properties adopted for the timber springs assuming a 127 mm fastener length and a 116 mm embedment length.

For the steel fastener, an elastic modulus of $k_{el} = 200000\ N/mm^2$ and yielding stress $f_y = 1103\ N/mm^2$ were adopted from [23] and [24]. A perfectly plastic behaviour was assumed for the fastener (i.e., $k_{pl} = 0\ N/mm^2$) with yielding stress used to parameterize the steel behaviour. A value of $a_1 = 20$ was selected to simulate an almost bilinear embedment behaviour, due to limited data for calibrating the transition curvature [19]. The expanded BoF model was applied to the connection configuration tested in the WOODWISE experiments to assess its viability to as a thermo-mechanical modelling strategy. Timber temperatures from the heat transfer analysis were used to determine char depths and progressively remove timber springs. To ensure numerical stability throughout the fire duration, a displacement-controlled analysis was adopted. A monotonic vertical displacement of 0.5 mm was imposed at the screw head over the entire duration of Test #3 (107 min).

3 RESULTS

3.1 Beam-on-Foundation model validation

The predictive capability of the proposed BoF formulation at ambient temperature was assessed against three independent experimental datasets covering a range of fastener diameters (8–12 mm), timber configurations (solid timber and CLT), and member thicknesses (60–90 mm), as summarized in Table 1. Figure 6 compares the predicted and validation embedment stress–displacement and force–displacement responses, with a Root Mean Square Error (RMSE) percentage relative to the maximum validation value per model.

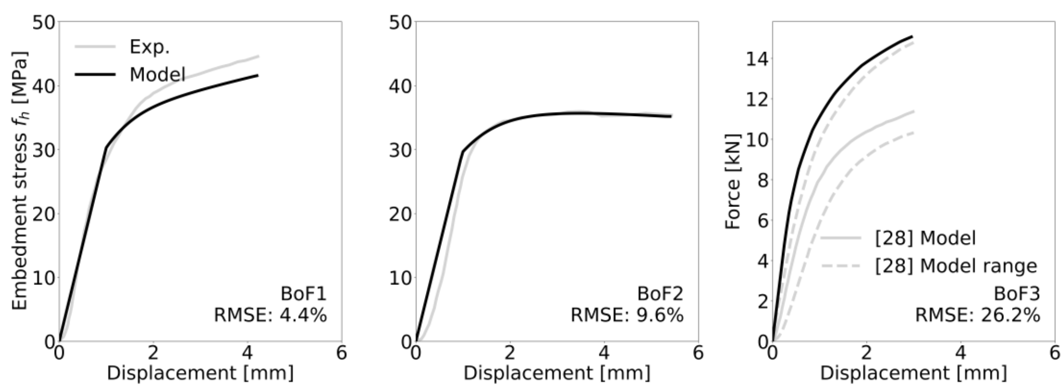

Figure 6. BoF ambient temperature model validation

Overall, the model reproduces the nonlinear response with good agreement. For BoF1 (8 mm, CLT), the predicted curve closely follows the experimental trend (RMSE = 4.4%). BoF2 shows larger deviations in the post-yield range (RMSE = 9.6%). For BoF3 (12 mm, CLT), the response aligns with the validated range in [26], with an RMSE of 26.2 %. The good agreement across different geometries and material configurations confirms the adequacy of the BoF model at ambient temperature.

3.2 Heat transfer model validation

Figure 7 presents the predicted temperature distribution at the end of Test #3 (107 min). The results show a thermal gradient from the exposed surface toward the interior of the CLT wall. A localized temperature increase is observed along the steel fastener embedment region, indicating enhanced heat penetration toward the steel element.

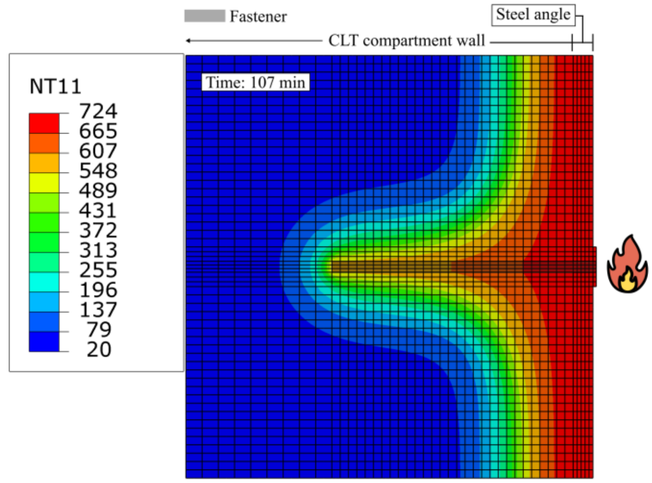

Figure 7. Heat transfer model results: Temperature distribution at the end of Test #3 fire.

Figure 8 compares predicted and measured temperature–time histories for Test #3 at depths from 0 mm to 124 mm from the exposed surface. The model simulates the overall heating trend at all monitored locations, including the rapid temperature rise near the exposed surface and the delayed response at greater depths. The largest discrepancies occur near the exposed boundary and at intermediate depths during rapid temperature increase. For locations further away from the fire exposed surface (60 mm and 73 mm), the model follows the measured trend, with differences primarily in the timing and rate of temperature increase. At 79 mm and 124 mm, both model and experimental results show reduced temperature levels, and the model captures the gradual increase throughout the fire duration.

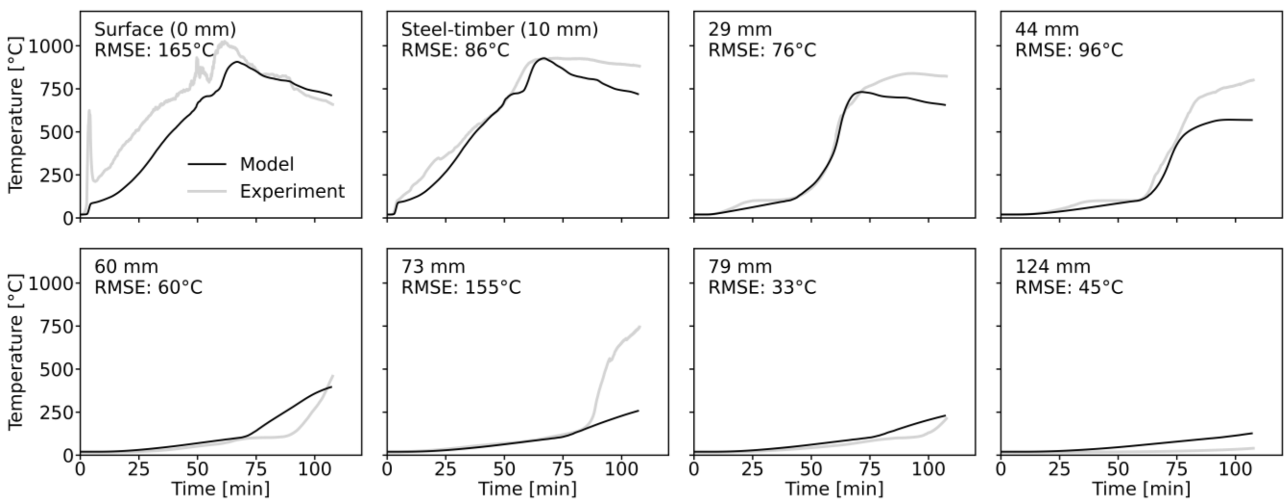

Figure 8. Heat transfer model validation against experimental dataset. Distance to exposed surface labelled in millimetres.

3.3 Expanded BoF model: Sequentially coupled thermal-stress analysis

Figure 9 presents the global force vs. vertical displacement response obtained from the sequentially coupled thermal-stress BoF analysis for Test #3. The reaction force initially increases with imposed screw head displacement, reaching a peak of approximately 0.40 kN, 47 minutes into the analysis, and corresponding to a char depth of 9 mm. This stage reflects the early heating phase, during which char depth has not progressed significantly.

Following the peak, a progressive reduction in reaction force is observed as displacement continues to increase. The force decreases steadily between approximately 50 and 70 minutes, coinciding with increasing char depth from 17 mm to 31 mm. This phase represents the onset of significant strength degradation of timber (and progressive removal of springs as they char).

Beyond 70 minutes, the response enters a lower reaction level. At 92 minutes (45 mm char depth), the reaction force reaches a minimum of approximately 0.08 kN. A slight increase is observed toward the end of the fire exposure (106 minutes, 52 mm char depth), associated with the imposed displacement and the progressive removal of timber springs. Overall, the reduction in global reaction force follows the computed increase in char depth and the corresponding removal of timber springs. Figure 10 presents selected deformed configurations, illustrating charring progression the resulting load transfer to the remaining uncharred springs. The model provides local vertical displacements of both timber springs and the fastener beam element. It also enables extraction of internal forces, stresses, and strains, including force–deformation responses of individual springs and axial stress–strain histories of the fastener, allowing assessment of screw bending and the onset of yielding leading to plastic hinge formation.

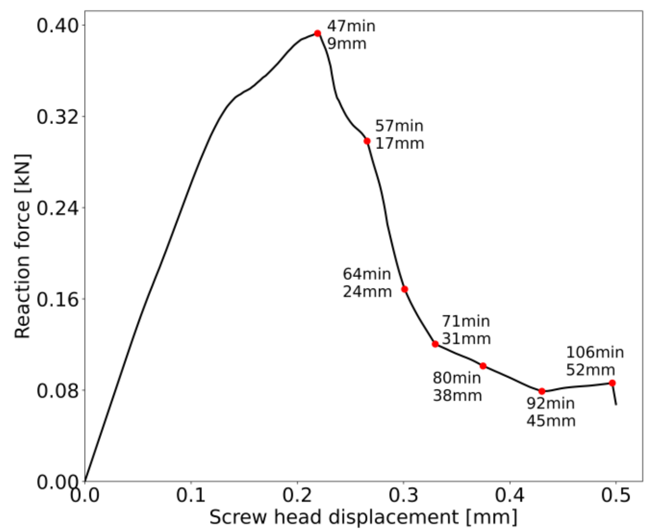

Figure 9. Expanded BoF model global response

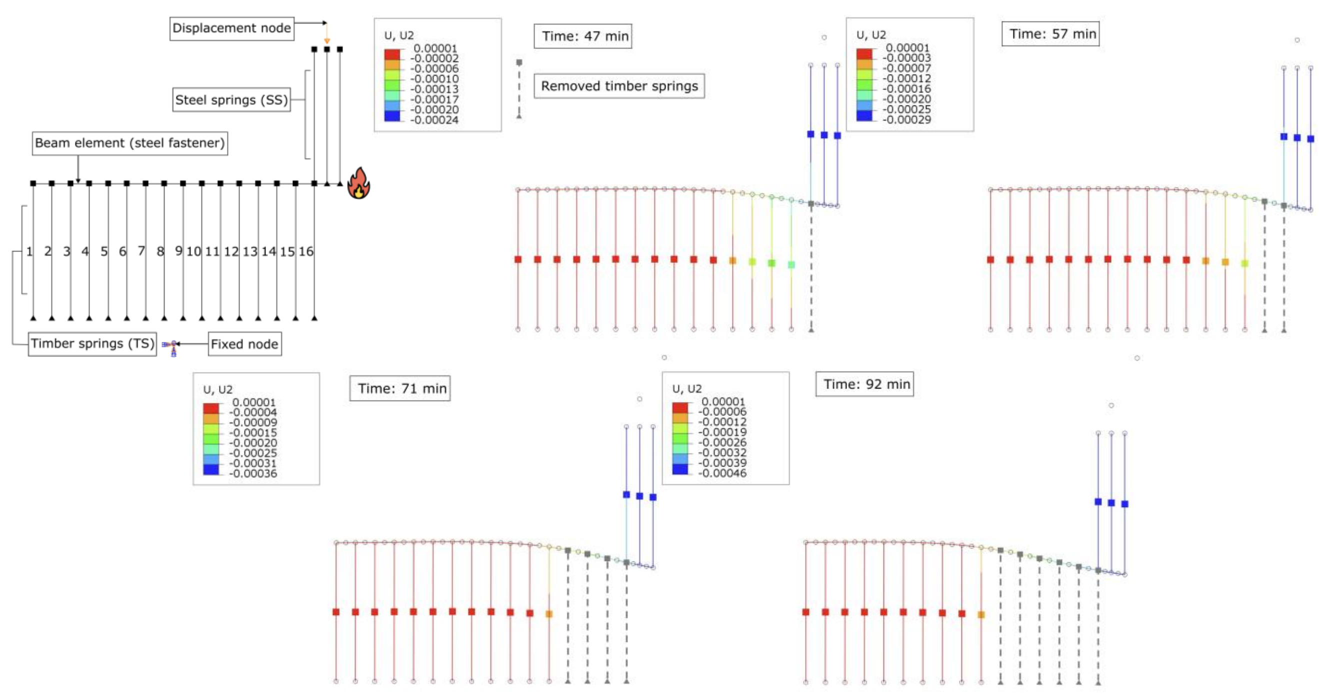

Figure 10. Expanded BoF model deformed shape during the analysis. Vertical displacement U2 in meters.

These outputs enable researchers to explore bending of the screw throughout the fire exposure as well as when the screw will begin to yield thereby approaching a plastic hinge.

4 CONCLUSIONS

This study developed a temperature-dependent BoF formulation for CLT balloon-frame connections exposed to the WOODWISE compartment fire. The work included heat transfer validation and a sequentially coupled thermal–stress analysis incorporating temperature-dependent degradation and progressive charring through modification and removal of timber springs.

Applied to WOODWISE Test #3, the model shows that the reduction in global reaction force follows the increase in char depth and corresponding spring removal. Beyond global force–displacement behaviour, the formulation enables extraction of local responses, including spring force–deformation histories and fastener stress–strain response, supporting evaluation of inelastic demand and load redistribution during fire exposure.

Limitations and Future work

Second-order (rope) effects and withdrawal resistance are not considered. Loading is assumed purely vertical, and the steel angle is treated as rigid. Temperature-dependent timber and steel properties from EC5 and EC3 are applied to a natural fire exposure; while common practice, this may not fully represent material behaviour under non-standard thermal histories.

Future work should extend the formulation to larger imposed displacements to capture fastener plastic hinging, incorporate withdrawal resistance and its interaction with shear, and include rope effects to assess axial force contributions at elevated temperatures. The model could also be generalized to larger-diameter screws and other dowel-type fasteners, such as dowels and bolts, through appropriate modification of embedment and fastener constitutive laws.

ACKNOWLEDGMENT

This research was funded by the National Institute of Food and Agriculture. C-REEMS Grant Proposal Number: 2022-08935; and the USDA Agricultural Research Services. TDI Proposal Number: USDA ARS 58-0204-4-002. The views expressed in this article are those of the author(s) and do not necessarily represent the views or policies of the U.S. Forest Service.

REFERENCES

1. Fischer, E. C., Bhandari, S., and Sinha, A. (2025). "Fire testing of glue-laminated beam-to-column connections." Journal of Structural Engineering, 151(4), 04025020. https://doi.org/10.1061/JSENDH.STENG-13888
2. Du Plessis, M., Streicher, D. & Walls, R. "Experimental Testing on Concealed Beam Hanger Mass Timber Connections Considering the Influence of Gap Size and Intumescent Sealants". Fire Technol 61, 5185–5210 (2025). https://doi.org/10.1007/s10694-025-01782-2
3. Frangi, A., Erchinger, C., and Fontana, M. (2010). "Experimental fire analysis of steel-to-timber connections using dowels and nails". Fire and Materials, 34(1), 1–19. https://doi.org/10.1002/fam.994
4. Fischer, E., Pitari, I., Hasburgh, L., Barber, D., Yedinak, K., and Coello, N. (2025). "WOODWISE: Large-scale compartment fire tests examining sustainability, smoldering, and emissions." Proc., World Conference on Timber Engineering, Brisbane, Australia.
5. Gikonyo, J. W., Schweigler, M., and Bader, T. K. (2024). "Beam-on-foundation modelling of dowel-type single fastener connections in cross-laminated timber." Engineering Structures, 303, 117519. https://doi.org/10.1016/j.engstruct.2024.117519
6. Hassanieh, A. (2016). "Load-slip behaviour of steel–cross laminated timber (CLT) composite connections." Journal of Constructional Steel Research, 122, 110–121.
7. Palma, P., Frangi, A., Hugi, E., Cachim, P., & Cruz, H. (2014). "Fire resistance tests on beam-to-column shear connections". In Proceedings of the 8th International Conference on Structures in Fire (SiF 2014), Shanghai, China, June 11–13, 2014.

8. Létourneau-Gagnon, M., Dagenais, C., and Blanchet, P. (2021). “Fire performance of self-tapping screws in tall mass-timber buildings.” Applied Sciences 11 (8): 3579. https://doi.org/10.3390/app11083579
9. Peng, L. (2010). Performance of heavy timber connections in fire. Ph.D. thesis, Carleton Univ., Ottawa, ON, Canada. https://hdl.handle.net/20.500.14718/31197
10. Erchinger, C., Frangi, A., and Fontana, M. (2010). “Fire design of steel-to-timber dowelled connections.” Engineering Structures 32 (2): 580–589. https://doi.org/10.1016/j.engstruct.2009.11.004
11. Marcolan Júnior, A. C., and Moraes, P. D. (2022). “Probabilistic model for determining the failure time of steel-to-timber connections with multiple dowel-type fasteners exposed to fire.” Fire Safety Journal 133: 103646. https://doi.org/10.1016/j.firesaf.2022.103646
12. Audebert, M., Dhima, D., Taazount, M., and Bouchaïr, A. (2011). “Numerical investigations on the thermo-mechanical behavior of steel-to-timber joints exposed to fire.” Engineering Structures 33 (12): 3257–3268. https://doi.org/10.1016/j.engstruct.2011.08.021
13. Audebert, M., Dhima, D., Taazount, M., and Bouchaïr, A. (2013). “Thermo-mechanical behaviour of timber-to-timber connections exposed to fire.” Fire Safety Journal 56: 52–64. https://doi.org/10.1016/j.firesaf.2013.01.007
14. CEN. (2004). “EN 1995-1-2: Eurocode 5: Design of timber structures – Part 1-2: Structural fire design”. European Committee for Standardization, Brussels, Belgium.
15. CEN. (1995). “EN 1993-1-2: Eurocode 3: Design of steel structures – Part 1-2: Structural fire design”. European Committee for Standardization, Brussels, Belgium.
16. Chuo, T. C. B. (2007). “Fire performance of connections in laminated veneer lumber”. MEFE thesis, Department of Civil Engineering, University of Canterbury
17. Palma, P., and Frangi, A. (2019). “Modelling the fire resistance of steel-to-timber dowelled connections loaded perpendicularly to the grain.” Fire Safety Journal 107: 54–74. https://doi.org/10.1016/j.firesaf.2017.12.001
18. Richard, R. M., and Abbott, B. J. (1975). “Versatile elastic-plastic stress-strain formula.”
19. Schweigler, M., Bader, T. K., Hochreiner, G., and Lemaître, R. (2018). “Parameterization equations for the nonlinear connection slip applied to the anisotropic embedment behavior of wood.” Composites Part B: Engineering 142: 142–158. https://doi.org/10.1016/j.compositesb.2018.01.003
20. Gikonyo, J. W., Schweigler, M., and Bader, T. K. (2024). “Exploring the relationship between embedment behaviour in cross-laminated timber and its layers: An experimental study.” Engineering Structures 318: 118677. https://doi.org/10.1016/j.engstruct.2024.118677
21. Hetényi, M. (1946). “Beams on Elastic Foundations”. University of Michigan Press, Ann Arbor, MI.
22. Schweigler, M., Bader, T. K., Bocquet, J.-F., and Lemaitre, R. (2019). “Embedment test analysis and data in the context of phenomenological modeling for dowelled timber joint design.” In Proceedings of INTER 2019, 6th Meeting of the International Network on Timber Engineering Research (INTER), Tacoma, WA, USA, September 2019.c
23. American Institute of Steel Construction (AISC). (2023). “Steel Construction Manual”, 16th Ed., Chicago, IL.
24. Simpson Strong-Tie. (2025). “Fastening Systems Technical Guide”, C-F-2025TECHSUP.
25. Schweigler M, Bader TK, Vessby J, Eberhardsteiner J. (2017). “Constrained displacement boundary condition in embedment testing of dowel-type fasteners in LVL”. Strain. 2017; 53:e12238. https://doi.org/10.1111/str.12238
26. Gikonyo, J. W., Schweigler, M., Bader, T. K. (2024). “Beam-on-Foundation modelling of dowel-type single fastener connections in cross-laminated timber”. Engineering Structures, 303, Article 117519. https://doi.org/10.1016/j.engstruct.2024.117519
27. Maia, B. B., Miotto, J. L., and Góes, J. L. N. de. (2021). “Embedding strength of fully-threaded dowel-type fasteners in cross-laminated timber: An experimental study.” Revista Matéria, 26(3), e13054.
28. Dong, W., Li, Q., Zhang, H., Wang, Z., Zhou, J., and Gong, M. (2019). “Embedment strength of cross-laminated timber for smooth dowel-type fasteners.” MATEC Web of Conferences 275: 01020. https://doi.org/10.1051/matecconf/201927501020
29. Lou, P., Zhang, X., Au, F. T. K., Zhang, Z., and Huang, Y. (2020). “A unified dimensionless parameter for finite element mesh for beams resting on elastic foundation.” Computer Modeling in Engineering & Sciences, 122(3), 955–969. https://doi.org/10.32604/cmes.2020.08302
30. Svensson, S., & Munch-Andersen, J. (2018). “Theory of timber connections with slender dowel type fasteners”. Wood Material Science & Engineering, 13(1), 7–15. https://doi.org/10.1080/17480272.2016.1226382
31. CEN (2023). Eurocode 5: Design of timber structures — Part 1-1: General rules and rules for buildings (prEN 1995-1-1:2023). European Committee for Standardization, Brussels, Belgium.